The Cryosphere Discuss., https://doi.org/10.5194/tc-2018-235
Manuscript under review for journal The Cryosphere
Discussion started: 7 January 2019

The Cryosphere Discussions

Distinguishing ice-rich and ice-poor permafrost to map ground temperatures and -ice content in the Swiss Alps

Robert Kenner[1], Jeannette Noetzli[1], Martin Hoelzle[2], Hugo Raetzo[3], Marcia Phillips[1]

[1] WSL Institute for Snow and Avalanche Research SLF
[2] University of Fribourg, Department of Geosciences
[3] Federal Office for the Environment FOEN

Correspondence to: Robert Kenner (kenner@slf.ch)

Abstract. A new countrywide permafrost distribution map of Switzerland is presented, indicating ground temperatures and ice content. The new representation of ground temperatures is achieved by distinguishing ice-poor and ice-rich permafrost in the modelling process. There is a very significant correlation of ground temperatures with elevation and potential incoming solar radiation in ice-poor and ice-free ground. The distribution of ice-rich permafrost was defined by modelling mass wasting processes and the integration of snow and ice into the ground caused by them. This dual approach allowed a clear improvement in the cartographic representation of permafrost-free elevational belts which are bordered above and below by permafrost. The reproduction of such commonly occurring permafrost gaps allowed a higher mapping accuracy and unambiguity of the mapping zones. Permafrost occurrence is represented by two clearly defined classes: Zone 1 representing modelled ground temperatures and zone 2 indicating excess ground ice outside of zone 1. 58% of 92 validation sites could be definitively classified as having permafrost or no permafrost. If only ice-poor or –free ground is considered, this value reaches 90%. The rather simple dependency of ice-poor permafrost on two main parameters is not only relevant for mapping but also for a wide range of scientific and engineering purposes.

The Cryosphere Discuss., https://doi.org/10.5194/tc-2018-235
Manuscript under review for journal The Cryosphere
Discussion started: 7 January 2019

1 Introduction

Maps of potential permafrost distribution are useful products applied in different fields of practice and research. They are used to plan construction work in alpine terrain, to evaluate local slope instability or to estimate large-scale permafrost occurrence for scientific purposes. An essential requirement for permafrost distribution maps is reference data to calibrate the permafrost model used. Such data are provided by monitoring networks such as the Swiss permafrost monitoring network PERMOS (2016), which was also used here. Previous approaches to map the entire permafrost in Switzerland (Deluigi et al., 2017;Böckli et al., 2012;Hoelzle et al., 2001;Keller, 1992;Keller et al., 1998;Gruber and Hoelzle, 2001;Gruber et al., 2006;Haeberli et al., 1996) are all represented by an empirical-statistical permafrost likelihood or index for different topographic settings and/or landforms. Predictor variables are typically mean annual air temperature (MAAT), represented by elevation and potential incoming solar radiation (Hoelzle and Haeberli, 1995). Further adjustment parameters are surface coverage, vegetation or topographic characteristics such as slope or curvature (Deluigi et al., 2017;Böckli et al., 2012;Hoelzle et al., 1993). These approaches have the advantage that uncertainties in the mapping of permafrost are clearly evident for the map user. However, the uncertainty in the prognosis of permafrost conditions are relatively high.

The permafrost and ground ice map (PGIM) of Switzerland presented here uses a different approach of mapping. Kenner and Magnusson (2017) and Kenner et al. (2017) highlighted the differences between ice-rich and ice-poor permafrost occurrence in terms of their development and conservation. Ice-rich mountain permafrost is considered as permafrost in talus ground containing excess ice and can therefore exist at places which do not allow the existence of ice poor permafrost. Such places refer mainly to the characteristic occurrence of ice-rich permafrost at the base of talus slopes (Haeberli, 1975). The origin of ground ice at places, unsuitable for ice-poor permafrost was explained by Kenner and Magnusson (2017) and Kenner (2018) with the burial of snow and ice by rock debris as dominant process, i.e. permafrost occurrence resulting from syngenetic ground ice formation. Other authors consider although the epigenetic development of segregation ice in talus slopes during colder climate periods as possible origin of current ice rich permafrost (Haeberli, 2000). Both processes are considered in this study.

The distribution of ice-poor permafrost (permafrost without excess ice) was focussed on as being controlled by air temperature and solar radiation (where limited amounts of ground ice exist, as a result of permafrost conditions). The important differences between ice-poor and ice-rich permafrost become apparent in the context of permafrost monitoring and process-based modelling. In general, ice-rich permafrost is less sensitive to climate fluctuations due to the thermal characteristics of ice and to latent heat effects (Scherler et al., 2013). In contrast to ice-poor permafrost, the active layer thickness of most ice-rich permafrost monitoring sites in the Swiss Alps remained stable during the last decades (PERMOS, 2016). However, if active layer thickening occurred, it was reversible in ice-poor permafrost (Krautblatter, 2009;Marmy et al., 2013;Hilbich et al., 2008), but irreversible in ice-rich permafrost due to the melt of considerable amounts of ground ice

(Zenklusen Mutter and Phillips, 2012). This highlights ground ice as a requirement for the existence of permafrost at such sites. Process-based permafrost modelling considers the deciding relevance of ground ice and relies on a soil stratigraphy including the ice content to reproduce accurate ground temperatures (Hipp et al., 2012;Staub et al., 2015;Pruessner et al., 2018). As ice content is typically considered for the purpose of process-based permafrost modelling it is logical to adopt this approach for permafrost mapping as well.

This differentiation between ice-poor and ice-rich permafrost is moreover the key to reproduce the permafrost-free elevational belt often occuring between ice-rich permafrost in lower elevations and ice-poor permafrost in higher elevations. Scapozza et al. (2011) point out that in all available permafrost models, the permafrost probability increases upslope, which is contradicted by their observations and by many other publications.

The PGIM presented here distinguishes between ice-rich and ice-poor permafrost and is therefore able to reproduce the inverse permafrost distribution described above. Furthermore, the different mapping approach of the PGIM allows the indication of modelled ground temperatures and areas with potentially high ground ice content, while existing permafrost maps represent a permafrost likelihood of occurrence instead. Our approach has not previously been implemented by other permafrost mapping studies and is applicable for mountain permafrost mapping worldwide. Here the PGIM is compared with existing permafrost maps of Switzerland.

2 Methods

The permafrost and ground ice map PGIM of Switzerland consists of two zones: Zone 1 indicates modelled ground temperatures and is based on the three parameters elevation, potential incoming solar radiation and slope. Zone 2 indicates areas outside of zone 1 which might be permafrost due to the existence of excess ground ice. The modelling approach for zone 2 differs completely from that of zone 1, instead of thermal effects, the potential existence of ground ice was considered here; either due to ground ice formation by mutual superimposing rock fall and snow avalanche deposits or due to the gravimetrical relocation of paleo excess ground ice.

2. 1 Mapping approach for zone 1

Zone 1 of the PGIM was derived from modelled ground temperatures. Zone 1 includes all areas with modelled negative ground temperatures and a buffer area with ground temperatures ranging between 0°C and 1°C. This buffer of 1 K corresponds to about the double standard error of our model output. The core area of zone 1 showing negative ground temperatures was labelled “Permafrost” and mapped in blue colours. The buffer area was mapped in yellow and is described as “possible patchy permafrost”. The ground temperatures were calculated based on a linear regression analysis using the explanatory variables potential incoming solar radiation and elevation (as a proxy for mean annual air temperature). Ground temperatures measured in 15 reference boreholes were used as predictor variables. These boreholes were chosen from areas without ice-rich permafrost (upper 15 sites in table 1). Temperature is measured in the boreholes at several depths by thermistor chains with a sub-day temporal resolution. The thermistors commonly have a measurement accuracy of around 0.1°C or better, the types of thermistor and data loggers are specified in PERMOS (2016).

The basic concept was to attribute a solar radiation value, an elevation value and a mean annual ground temperature to each of the 212 thermistors. Based on this dataset, the regression parameters a, b and c in formula 1 were determined and later used in formula 3 (together with an elevation and insolation model) to calculate the ground temperatures in zone 1.

$$MAGT = a + b \cdot R + c \cdot E \qquad (1)$$

Where:

MAGT is the mean annual ground temperature at each single borehole thermistor
R is the solar radiation value for each single borehole thermistor
E is the elevation of each single borehole thermistor

Attributing a MAGT to each thermistor is straightforward. To attribute solar radiation values and elevation we created a point cloud representing the ground surface around each borehole, in which every point contained information on its elevation and potential solar radiation. The points were categorized into distance classes with 1 m increment, dependent on their distance to an individual thermistor. Elevation and solar radiation values of surface points surrounding each thermistor where then aggregated by calculating a weighting average based on the inverse distance thermistor – surface point and the amount of points within one distance class (see formula 2). The maximal distance between thermistors and surface points considered was 5 times the minimal distance of the thermistor to the ground surface. This factor was optimized empirically.

$$R = \frac{\sum_{i=n}^{i=1} d_i \cdot r_i \cdot k_i}{n} \qquad (2)$$

Where:

R is the solar radiation value defined for a single borehole thermistor
n is the number of distance classes
d is a weighting factor which considers the distance between a surface point and the thermistor (inverse distance weighting)
k is a weighting factor which considers the number of surface points within one distance class
r is the solar radiation value of a single surface point

Potential incoming solar radiation of every surface point was calculated with the ESRI tool “Area solar radiation” with the parameter transmissivity set at 0.4, and diffuse proportion at 0.5, which corresponds to values recommended for moist temperate climates by the software developer. The snow cover can strongly influence the solar radiation budget. Most of the alpine ground surface is snow covered for at least 6 months and receives no insolation during that time. However, steep areas such as rock walls remain snow free for the entire year. To consider the snow cover in slopes below 40°, we only used solar radiation values calculated for the generally snow-free period July to November.

Defining solar radiation values for slopes steeper than 40° was more difficult. Solar radiation is just one component of the radiation balance and our simplified model does not consider its counterpart, the long-wave emission. This however is a critical parameter during the winter period in steep snow free areas such as rock walls. In our model, any additional winter insolation on snow free surfaces would lead to a warming of the snow free ground on an annual basis. This might be correct

The Cryosphere Discuss., https://doi.org/10.5194/tc-2018-235
Manuscript under review for journal The Cryosphere
Discussion started: 7 January 2019

for steep southern slopes where winter insolation causes a positive feedback of warming. Firstly, it causes snow removal due to melt or the triggering of wet avalanches and subsequently an effective heating of the bare ground above the mean air temperatures (Haberkorn et al., 2015a). In steep, snow free northern slopes however, the opposite occurs. Long-wave emission clearly dominates the radiation balance here, causing rock surface temperatures close to or even below the air temperatures (Haberkorn et al., 2015a). To overcome this weakness, the winter insolation (December to July) which affects the steep terrain parts was multiplied with an empirically defined aspect-dependent factor. This factor ranges between 0 for the azimuth North (no effect of winter insolation due to similar strong long-wave emission) and 1 for the azimuth South (strongest effect of winter insolation). The winter solar radiation was then added to the summer solar radiation values and applied to slopes steeper than 40°.

The intention of the PGIM was to include almost all ice-poor permafrost within zone 1. To meet this requirement, we had to consider the spread within the regression result. The temperature of single thermistors can deviate from the regression line towards warmer or colder conditions for reasons analysed in the discussion section. To include deviations towards lower temperatures, the regression analysis was carried out twice. While all thermistors where used in the first iteration, only those thermistors whose measured MAGT lay below the modelled MAGT in the first iteration were used in the second iteration.

To set up the regression model the input parameters solar radiation and elevation were computed with the maximal available resolution of 2 metres around each borehole (based on Swisstopo swissALTI3D). To produce the map, the regression result was applied to a digital elevation and insolation model with 25 m resolution (DEM25 and DIM25, based on Swisstopo DHM25). Hereby, the temperature value of each 25 m raster cell of the PGIM was defined by:

$$PGIM_{zone1} = 17.275 + 4.059 \cdot 10^{-6} \cdot DIM25 - 0.007015 \cdot DEM25 \quad (3)$$

This implies that depth-dependent 3D effects, which were considered by the inverse distance weighting in our regression model, are not included in our map. In fact, such effects lose significance due to the lower resolution of the map in which insolation variations are spatially averaged within a 25 m raster cell. The temperatures in the map can therefore be interpreted as the 3D spatial average of mean annual ground temperatures within one raster cell.

2.2 Sensitivity analysis of the regression result

The regression result depends on the following parameters: potential incoming solar radiation, elevation, reference ground temperatures and distance threshold. Changes in these parameters will influence the regression result. Elevation is a well-known value which is independent from external influences and therefore uncritical for the regression result. Reference ground temperatures can be influenced by environmental conditions, which are not considered here as well as by measurement errors. A small to medium size statistical sample of measured ground temperatures might therefore be distorted in comparison to the total statistical population. To test the sensitivity of our result to changes in the statistical sample we recalculated the results with a randomly bisected sample of reference boreholes. We then compared the modelled ground temperatures of all 212 thermistors based on the entire set of reference temperatures with the modelled ground temperatures based on the bisected set of reference temperatures.

The Cryosphere Discuss., https://doi.org/10.5194/tc-2018-235
Manuscript under review for journal The Cryosphere
Discussion started: 7 January 2019

The calculation of solar radiation values, especially in steep terrain, included several other parameters such as a slope threshold, an aspect-dependent weighting factor and assumptions for the timing of snow coverage. Indeed, the model was optimized by applying these parameters. The solar radiation values as well as the distance threshold are however not an independent statistical unit of a sample of observations but are all based on the same calculation. They are therefore not the origin of random changes in the regression result.

2.3 Testing the mapping approach of zone 1 for zone 2

A second regression analysis was set up including ice-rich permafrost boreholes. The aim was to investigate changes in the regression result in dependency of the ice content of the reference boreholes. Here we used a simplified version of the approach described above. We only used the thermistor with the lowest temperatures (indicator for permafrost) in each borehole and the elevation and insolation values directly at the borehole. To minimize the effects of 3D heat conduction we only used data from boreholes in homogeneous slopes and not from ridges.

2.4 Finally applied mapping approach for zone 2

Zone 2 includes all forms of ice-rich permafrost such as rock glaciers or ice-rich talus slopes. The basic concept was to define areas in which the burial of ice or snow by rock fall can lead to the development of ground ice or at which epigenetic ground ice could have been relocated due to ground deformation processes.

First the hydrological flow accumulation lines from rock walls steeper than 40° were defined in ERSI ArcGIS on the basis of a 25 m DEM. This was done in areas above 2000 m a.s.l., as only few, azonal permafrost sites exist below (Cremonese et al., 2011). The runoff tracks were buffered by a 120 m wide belt (empirically optimized value) and in their upper parts the resulting strips correspond to the main tracks of snow avalanches and rock fall. Further downslope they represent potential rock glacier creep paths. These areas were then reduced stepwise by excluding spatial intersections with other datasets, namely:

- All areas steeper than 30° (based on “DHM25” provided by Swisstopo), which have been shown to barely contain ice rich permafrost (Kenner and Magnusson, 2017). This might be because snow avalanches seldom form deposits in such steep slopes and epigenetic segregation ice would leave steeper slopes by the initialisation of creep processes.
- All vegetation-covered areas because they commonly consist of fine-grained soils at relatively low elevations, where ice-rich permafrost is generally absent in the European Alps (Hoelzle et al., 1993). The vegetation coverage was deduced from orthophotos (“SWISSIMAGE” provided by Swisstopo) using the SAVI Index (Huete, 1988). Areas of vegetation / no vegetation within the resulting 25 m grid were homogenized by iteratively applying a classic 3x3 cell erosion and dilation operation.
- Flood plains, which were defined as being areas with slope < 4° and intersected by rivers (based on “DHM25” and “swissTLM3D” provided by Swisstopo).
- Lakes and glaciers (based on “swissTLM3D” provided by Swisstopo)

- Maximal extents of Little Ice Age (LIA) glaciation, because glacier coverage is known to disrupt underlying permafrost (Ribolini et al., 2010;Reynard et al., 2003). This dataset was created by Maisch (1999).

The remaining polygons were then aggregated to fill small gaps, simplified and smoothed. After this, all areas listed above were again excluded from the reworked polygons.

In a final step, the resulting polygons were checked and if necessary edited manually. Some of them still contained areas in which bedrock at the surface excludes the development of ice-rich permafrost development as described above. In a few cases, parts of rock glaciers were missing due to errors in the reproduction of creep paths or due to small terrain steps with slopes over 30°. Manual editing included two tasks: All areas showing a bedrock surface, infrastructure or > 50% vegetation coverage (which was for some reason not captured by the SAVI index) were removed from zone 2. Missing parts of rock glaciers were added to zone 2 if at least parts of them were already captured by the automatic mapping approach. The polygon editor was not aware of the positions of the validation points during this process.

Zone 1 and zone 2 provide two different types of information: Zone 1 indicates ground temperatures based on a simplified surface energy balance. Zone 2 indicates areas of potential ground ice existence of different sources, which can lead to the occurrence of permafrost outside the thermally based zone 1. Both zones can overlap and zone 1 was mapped with the higher priority here; firstly because it has the higher mapping accuracy and secondly zone 2 was intended as supplement to zone 1 to solve the problem of permafrost occurrence that is hard to explain thermally. This implies that ice-rich permafrost can also occur within zone 1, where it is not distinguished from ice-poor permafrost.

3 Validation

The permafrost map was validated using a set of 92 evidence points of permafrost occurrence or permafrost absence. A more detailed verification, e.g. of modelled temperatures, was not possible due to the lack of data. Some of these validation points correspond to the dataset collected by Cremonese et al. (2011). Records from this database were only used if they have exact coordinates and show direct evidence of permafrost occurrence or absence; either based on observations of ice in construction work trenches and rock fall scars or based on ground temperature data measured in boreholes.

Of the records in this database, 74 % indicate permafrost. To include more non-permafrost validation points we added a second validation dataset based on continuous ground surface temperature data (GST) measured at 38 automatic weather stations in the Intercantonal Measurement and Information System (IMIS) (Russi et al., 2003). To balance the number of validation points with and without permafrost, only IMIS stations above 2400 m elevation were used, which turned out to be most relevant for validation purposes as they lie within the critical elevation belt of discontinuous permafrost. These IMIS stations measure ground temperature within the uppermost 10 cm with a Campbell 107 temperature probe. Of these 38 IMIS stations, 33 register a constant zero curtain during winter and are therefore on permafrost-free ground (Hoelzle, 1992). The remaining 5 stations show quite constant winter GST between -3°C and -4°C and are located on active rock glaciers. They

The Cryosphere Discuss., https://doi.org/10.5194/tc-2018-235
Manuscript under review for journal The Cryosphere
Discussion started: 7 January 2019

were therefore classified as permafrost sites. Furthermore, a few additional borehole sites, which are not included in Cremonese et al. (2011) were added to the validation set (Table 2).

All classes of the PGIM were attributed with the number of validation records lying within them indicating permafrost occurrence or permafrost absence. The same validation process was applied to the alpine permafrost index map (APIM) created by Böckli et al. (2012) and the potential permafrost distribution map (PPDM) created by Gruber et al. (2006), available online in the Swisstopo web map service (Swisstopo, 2018). A closer methodical background to the PPDM can be found in Haeberli (1975), Keller (1992) and Gruber et al. (2004). Additionally, zone 2 of the PGIM was validated against a rock glacier inventory of the Albula Alps created by Kenner and Magnusson (2017). With 124 records, the inventory represents all rock glaciers in the 361 km^2 large alpine zone (area above 2000 m a.s.l.) of the Albula Alps.

4 Results

Predicting the ground temperatures of the ice-poor reference boreholes on the basis of elevation and potential incoming solar radiation yields a correlation coefficient of 0.94 and a standard error of 0.57°C (Table 3, Fig. 1). The regression result highlights the strong dependency of ice-poor permafrost on elevation (MAAT) and solar radiation and underlines its relatively high predictability. Although thermistors of individual boreholes show clear deviations from the regression line, bisecting the set of reference temperatures had limited effects on the regression result. The differences between the modelled ground temperatures based on the entire set of reference temperatures and the ground temperatures based on the bisected sample showed a mean value of -0.11° C and a standard deviation of 0.15 °C. The largest deviation found for a single thermistor was 0.51° C. The similar values for the standard deviation and the mean value suggest that the changed reference sample mainly caused a constant offset of the temperatures of slightly over -0.1° C. Transferred into the map, this corresponds to an elevation shift of zone 1 by about 12 m. Explanations for the deviations of single boreholes or thermistors are discussed later. Including ice-rich permafrost in this regression analysis causes a drastic drop in the predictability of permafrost (Table 3 and Figure 2). The formerly strong correlation practically disappears.

The Cryosphere Discuss., https://doi.org/10.5194/tc-2018-235
Manuscript under review for journal The Cryosphere
Discussion started: 7 January 2019

The Cryosphere Discussions
Open Access
EGU

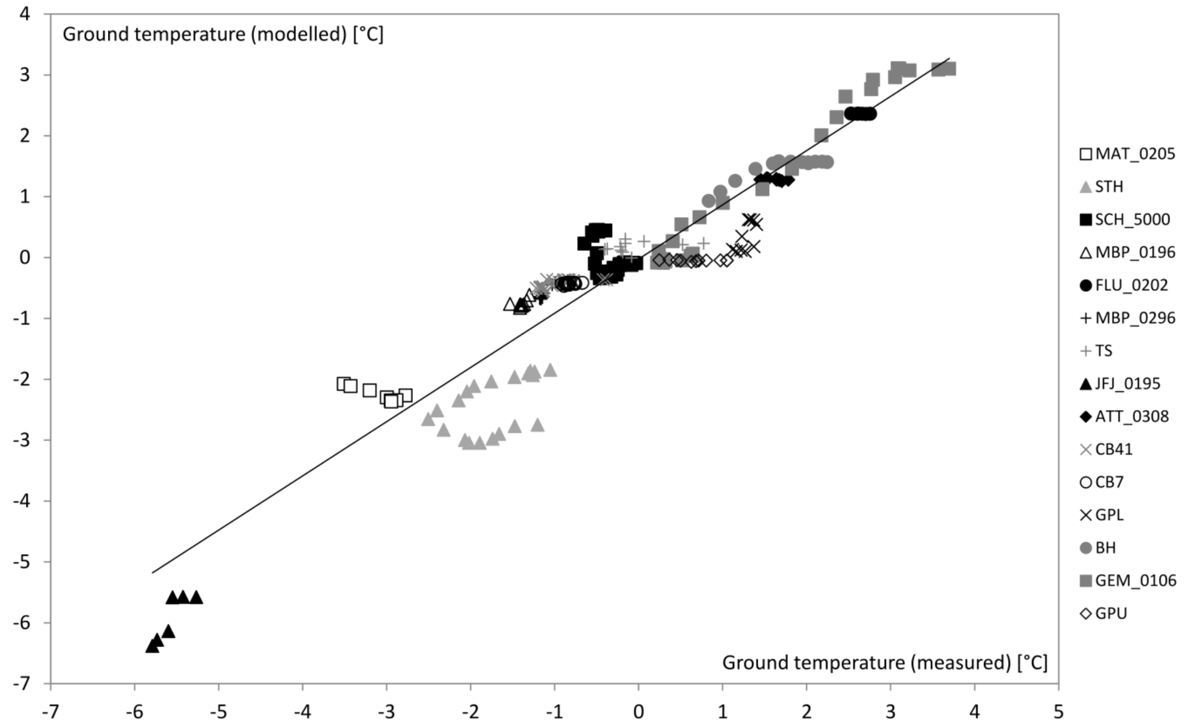

Figure 1: Measured MAGTs in 15 boreholes plotted against the modelled MAGT at the same locations. The regression line corresponds to formula (3) given in section 2.1. The borehole abbreviations are explained in table 1.

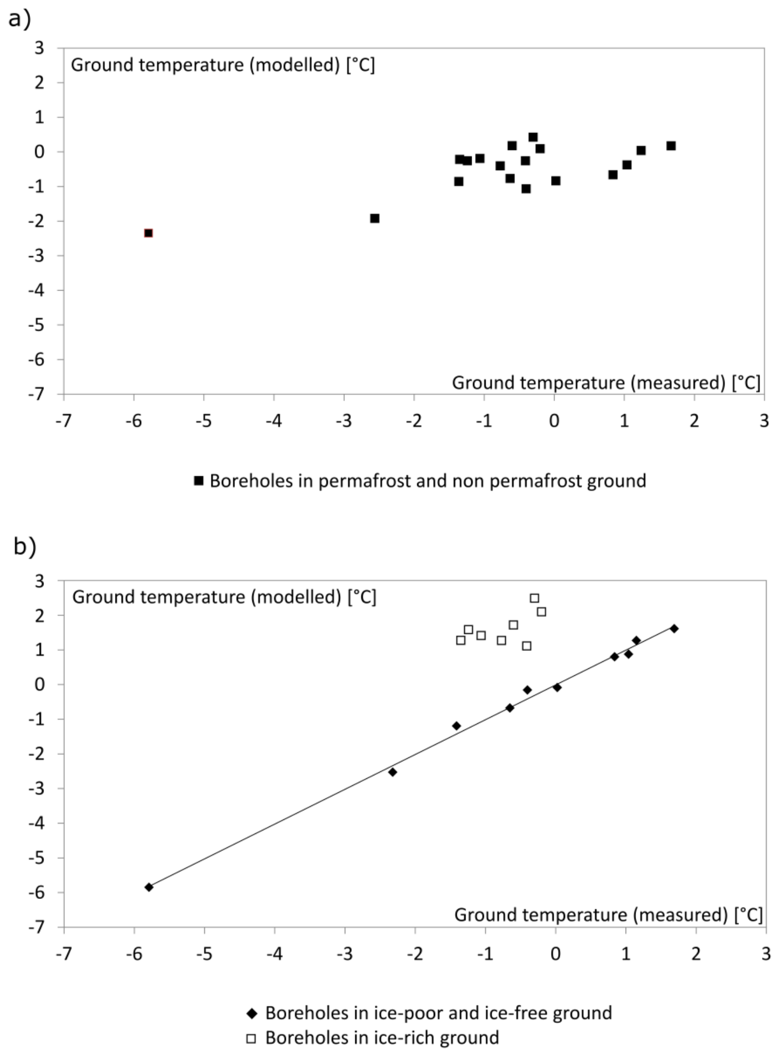

Figure 2: Each data point represents a borehole and its measured and modelled mean annual ground temperatures at the depth with lowest temperatures. Included are the ice-poor boreholes 1-10 and all ice-rich boreholes in Table 2. The linear regression based on elevation and potential solar radiation shows no systematic relation between these two parameters and the ground temperatures when using both ice-poor and ice-rich boreholes for the regression (a), but a clear correlation appears when using only ice-poor or ice-free boreholes (b).

The validation of the PGIM (Fig. 3) confirms the high accuracy of ice-poor permafrost prediction. Twenty of 22 validation sites representing ice-poor permafrost are located in the core area of zone 1 "permafrost" (modelled negative ground temperatures), one validation point in the buffer area of zone 1 "possible patchy permafrost" and one site outside the permafrost zonation. In turn, 0 of 49 sites devoid of permafrost were located in the core area of zone 1, and 4 in the buffer area of zone 1. Zone 2 (potential ice-rich permafrost) includes 31 sites indicating permafrost and 2 indicating permafrost absence. Zone 2 furthermore includes 95.5% of the rock glacier area registered in the Albula Alps inventory (Kenner and

Magnusson, 2017). This value applies to the automatically created version of zone 2 before it was manually edited and some rock glacier outlines were redrawn. The PGIM is available online as shapefile https://doi.org/10.5281/zenodo.1470165.

The validation of the APIM (Boeckli et al. 2012) is shown in Figure 4. The two zones representing "No permafrost" and the highest permafrost probability have a similar error rate as the corresponding classes in the PGIM, but contain less validation records. For the remaining classes the permafrost distribution over the indices is rather homogeneous except for the very high indexed areas (> 80) where an increase in permafrost frequency is visible.

The validation result of the PPDM (Gruber et al. 2006) is shown in Figure 5. The different probability ranges reflect the actual permafrost frequency quite well for the high probability classes but show some larger deviations for the lower classes. Several permafrost evidences exist outside the permafrost zonation of this map.

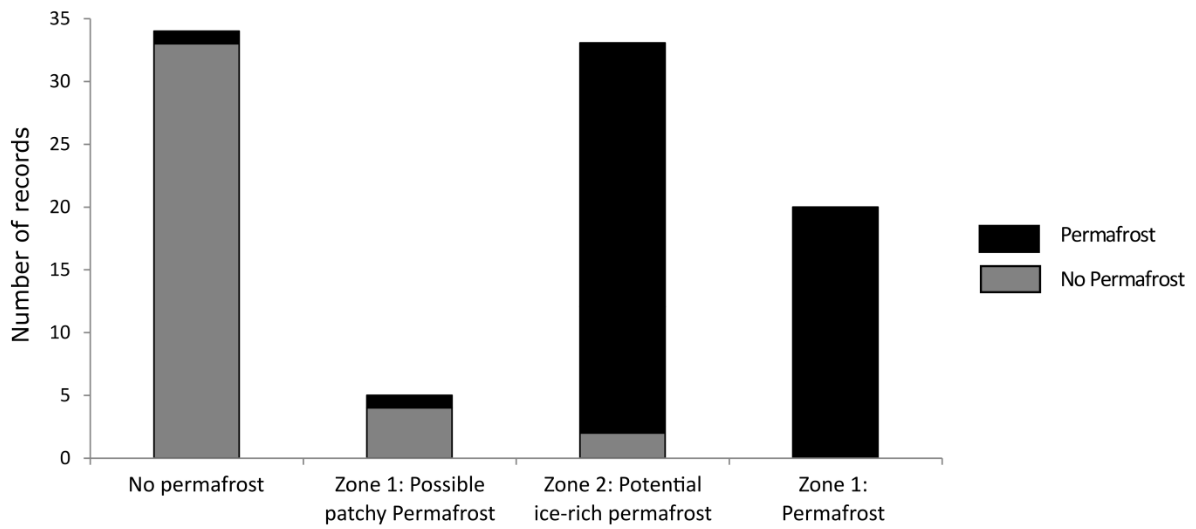

Figure 3: Validation of the PGIM showing the number of sites with permafrost occurrence and permafrost absence in each map class.

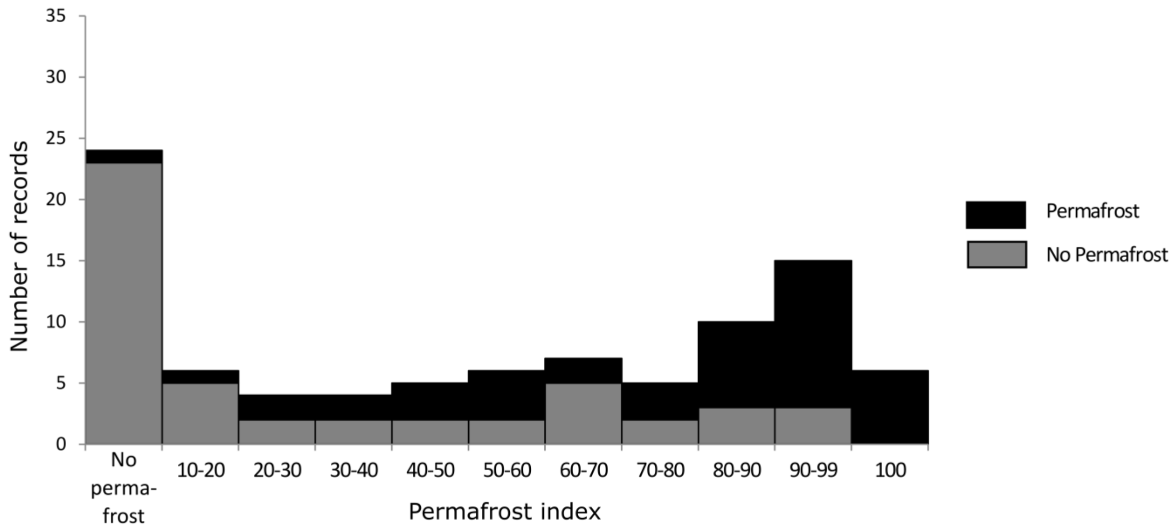

Figure 4: Validation of the APIM (Boeckli et al. 2012) showing the number of sites with permafrost occurrence and permafrost absence for different permafrost probability ranges. As the map does not define classes but gives unique index values for each cell of the map, ranging from 0.1 to 1, these values were classified in 10 permafrost classes and a "No permafrost" class including all records outside the permafrost zonation.

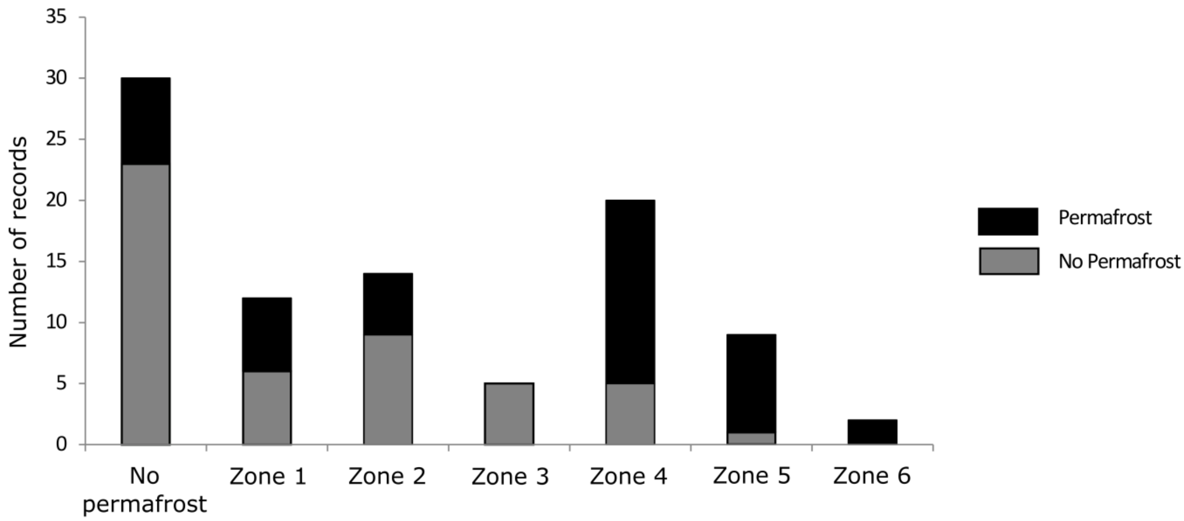

Figure 5: Validation of the PPDM (Gruber et al. 2006) showing the number of sites with permafrost occurrence and permafrost absence in each map class. The zones were originally defined as follows: Zone 1 – local permafrost possible, patchy, discontinuous; Zone 2 - local permafrost possible, frequent patchy distribution; Zone 2 - local permafrost possible, patchy to extensive; Zone 4 – Extensive permafrost likely; Zone 5 – Extensive permafrost likely, increasing thickness; Zone 6 – Extensive permafrost likely, very thick in places, to over 100 m. The class "No Permafrost" includes all records outside the permafrost zonation.

The Cryosphere Discuss., https://doi.org/10.5194/tc-2018-235
Manuscript under review for journal The Cryosphere
Discussion started: 7 January 2019

5 Discussion:

5.1 Permafrost predictability

The large deviations of the temperature data acquired in ice-rich permafrost within our regression model (table 3, column 4) highlights the importance of distinguishing between ice-rich and ice-poor permafrost. The high correlation coefficient achieved when using only ice-poor permafrost in the regression model is remarkable, in particular when taking into account that the borehole temperatures represent different landforms with strong differences in substrate and snow coverage. These factors, which are known to influence ground temperatures (Haberkorn et al., 2015b;Zhang, 2005;Hoelzle and Gruber, 2008), are represented in the regression result by rather small deviations of less than 1 K (Figure 6).

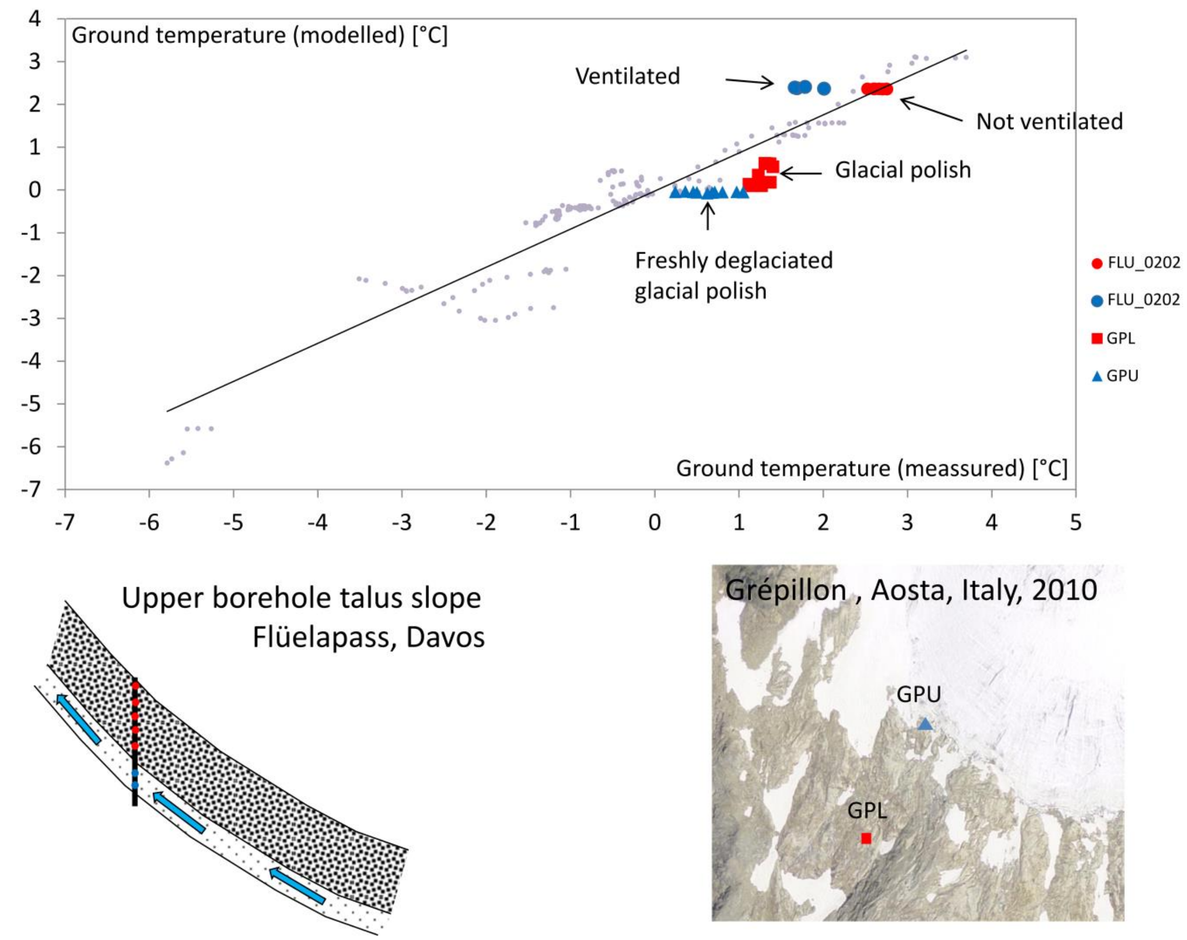

Figure 6: The Flüela- and Grépillon boreholes show nice examples of thermal disturbances. The lowermost 3 thermistors in Flüela (FLU_0202) are ventilated (Phillips et al., 2009) and thus deviate from the regression line. The Grépillon boreholes are drilled in a glacial polish, which can warm more efficiently than the loose rock surfaces at most of the other boreholes. The upper Grépillon borehole (GPU) was just recently deglaciated: whereas the uppermost thermistors have adapted to the new thermal conditions,

there is a clear temperature gradient towards lower temperatures at greater depth. Here, the temperatures are still close to 0° C as a consequence of the former glaciation.

Nevertheless, such disturbing effects are clearly visible in some cases. Figure 6 shows examples of thermistors which deviate from the regression line due to advective cooling (Flüelapass, (Phillips et al., 2009)), substrate characteristics (relatively warm glacial polish at the lower Grépillon borehole) or temperature disturbances due to former glaciation (upper Grépillon borehole).

The high predictability of ice-poor permafrost is insufficiently exploited when ice-rich permafrost is not treated separately in the data analysis (Table 3 and Figure 2). Ice-poor and ice-rich permafrost have different thermal regimes, mechanisms of conservation and rates of degradation, and must therefore be distinguished in permafrost modelling, mapping or climate sensitivity analyses. The predictability of ice-rich permafrost is clearly lower and requires the consideration of mass wasting processes such as rock fall, avalanche activity and varying glaciation during the entire Holocene. The accurate cartographic representation of these processes is therefore limited.

5.2 Map interpretation, uncertainty and accuracy

In contrast to other maps, the PGIM only has 2 zones, which are simple to interpret: Zone 1 represents modelled ground temperatures and zone 2 specifies areas with potentially high ground ice content caused by mass movement processes (Fig. 7). This approach reduces the mapping uncertainty while preserving a high accuracy.

The uncertainty can be quantified by the validation points, which are clearly attributed by the map as being permafrost or not. In the PGIM, definitive permafrost is indicated by the core area of zone 1. In the APIM definitive permafrost is indicated by a permafrost index of 1 (for validation, values higher than 0.994 were rounded to 1). The PPDM does not have a zone of definitive permafrost. Definitive permafrost absence is indicated on all three maps for areas outside the permafrost zonation. Compared to the other maps, the PGIM can attribute the most validation points to a definitive class, indicating either permafrost occurrence or permafrost absence (Figures 3-5).

Accuracy can be measured by the number of validation points wrongly attributed to a definitive class or by the plausibility of the description of a class. In the PPDM 7 permafrost sites occur outside the permafrost zonation. The definitive permafrost classes of the APIM and the PGIM predict all validation points contained within them correctly - with the exception of one site (Emshorn-Oberems), which was attributed wrongly on both maps. A general problem that is hard to quantify is the bias in both, the validation dataset and the reference boreholes. Terrain form and geographical location of these sites are not a balanced representation of the natural variability. Terrain or region related errors of the permafrost reproduction, which are not captured in this accuracy analysis are therefore possible.

The APIM includes almost all areas in Switzerland in which permafrost will occur and is therefore a useful tool to exclude permafrost at a certain location. However, similar to the PPDM it shows weaknesses in the reproduction of permafrost-free areas, while PGIM performs better here. This might be caused by the 'elevational permafrost gap' phenomenon. In the Alps

The Cryosphere Discuss., https://doi.org/10.5194/tc-2018-235
Manuscript under review for journal The Cryosphere
Discussion started: 7 January 2019

The Cryosphere Discussions

permafrost distribution is commonly characterised by thermally induced permafrost in the upper parts of a rock wall, with a ‘permafrost gap’ below, and ice-rich permafrost at the base of the underlying talus slopes. Figure 8 shows the example of the research site Flüelapass (Kenner et al., 2017), showing this pattern of permafrost distribution.

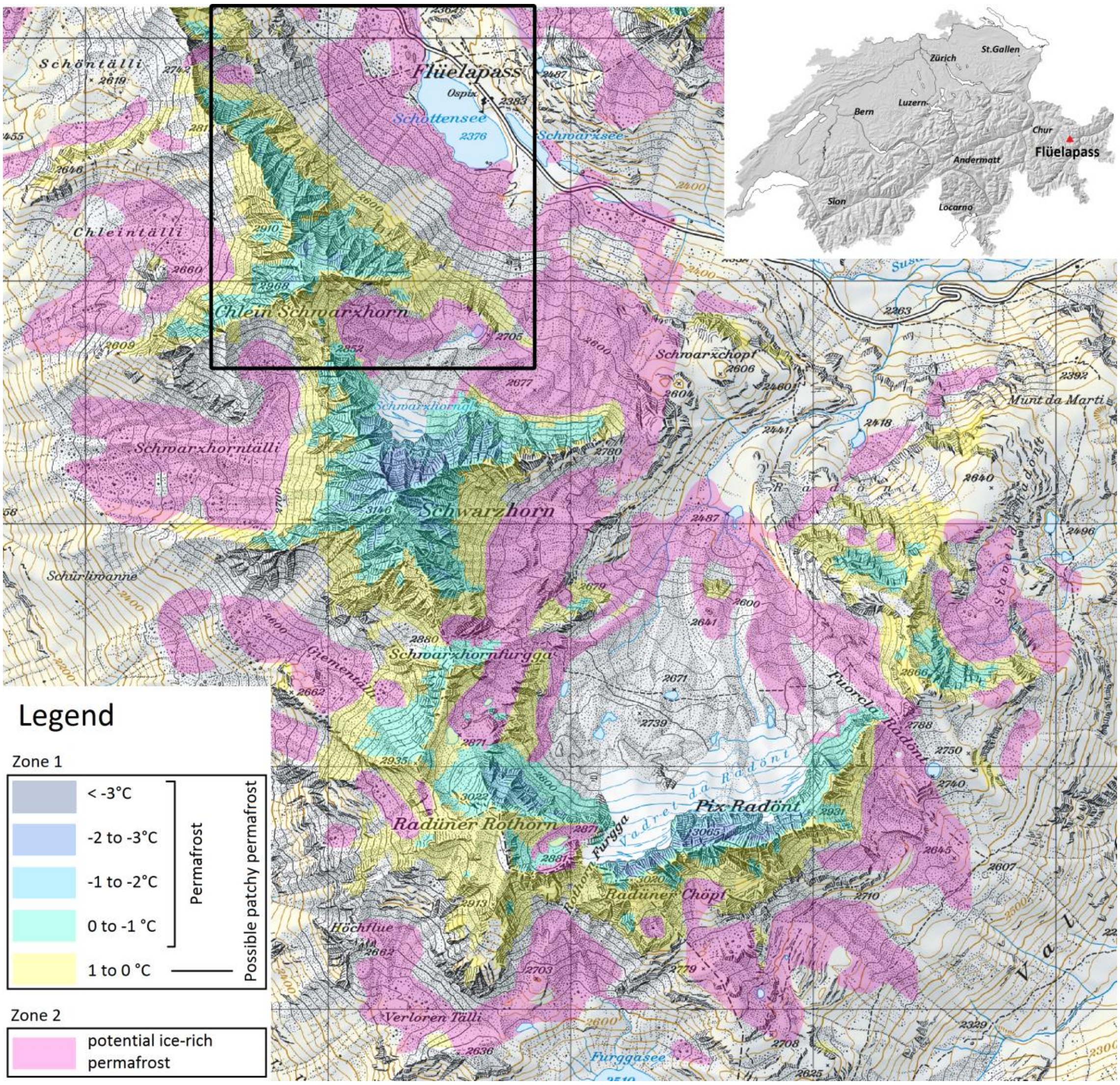

Figure 7: Map section of the PGIM close to Flüelapass, showing the permafrost distribution in two zones. The black frame is the sector shown in Fig. 8. The map grid has a resolution of 1 km. (Map: pixmaps © (2017) swisstopo (5704 000 000))

Mapping solely based on thermal influences does not reproduce the permafrost gap and either neglects the permafrost at the base of the talus slope (Fig. 8b) or overestimates the permafrost further upslope (Fig. 8b and 8c). This problem leads to peaks of permafrost absence in the zones of medium permafrost probability on the comparison maps. For example, the 60-70 % probability zone on the APIM or the zone “local permafrost possible, patchy to extensive” on the PPDM (Figures 4 and 5).

This may also cause the rather random distribution of permafrost-free validation points over the remaining probability classes of the APIM. In the PGIM the permafrost gap becomes visible when plotting the mapped permafrost area against elevation as shown in Figure A (supplementary material). A more accurate identification of this permafrost gap is an important step because it enables a better planning of infrastructure construction projects in alpine terrain.

The typical azonal permafrost found at low elevations (<2000 m), at sites like Creux du Van (Delaloye et al., 2003) or Dreveneuse (Delaloye and Lambiel, 2007) is not included on any of the permafrost distribution maps for the Swiss Alps discussed in this paper. The presence of azonal permafrost is possible due to a constellation of processes involving unusually effective advective cooling. These are difficult to implement in a large-scale map.

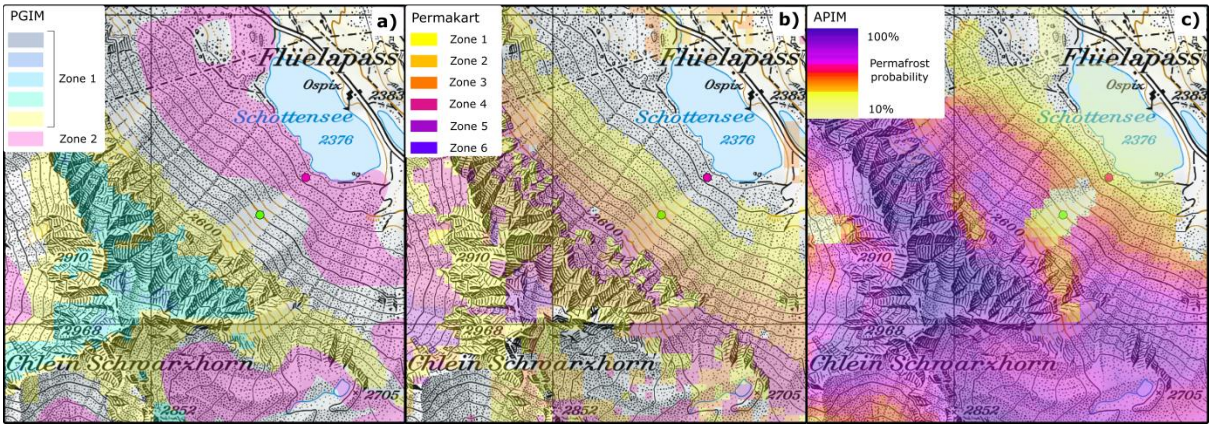

Figure 8: Comparison of three permafrost maps at the research site Flüelapass (a: PGIM, b: PPDM (Gruber et al. 2006), c: APIM (Boeckli et al. 2012)). This example shows typical alpine permafrost distribution, with ice-rich permafrost at the base of a talus slope, a permafrost gap further upslope and permafrost in the rock wall above the talus slope. A borehole without permafrost (green dot (FLU_0202)) is located in the permfrost gap, another with ice-rich permafrost (pink dot (FLU_0102)) is located at the base of the slope. (Map: pixmaps © (2017) swisstopo (5704 000 000))

5.3 Challenges and possible future approaches in mapping ice-rich permafrost

The ice-rich permafrost in zone 2 of the PGIM has a relatively high uncertainty. The low number of permafrost-free validation points (2 out of 33, see Fig. 3) here might rather overestimate the accuracy of this zone due to a general lack of permafrost-free validation points in talus slopes. However, there is very little ice-rich permafrost outside this zone, as indicated by the 95% representation of the Albula rock glacier inventory within the automatically created raw version of zone 2. Accordingly, zone 2 should not be interpreted as a reliable representation of ice-rich permafrost but rather as a best-possible one including most of the ice-rich permafrost in Switzerland, with some bycatch of permafrost-free ground. This area needs to be narrowed down in a common effort by the permafrost community and improved updates of the map are planned in future. This has certain challenges, which are discussed below.

Rock glaciers are a clearly visible indicator of ice-rich permafrost but are also the most critical ice-rich permafrost features to map, as the creep process has to be considered. Creep paths are sometimes hard to reproduce, as rock glaciers change the terrain morphology in such a way that the runoff tracks, which are the basis of zone 2, run laterally to the convex rock glacier body and their buffer zone does not incorporate the whole rock glacier. Additionally, in some cases rock glaciers creep over terrain steeper than 30° and these parts of rock glaciers are missing in zone 2. A further problem is caused by rock glaciers mapped as LIA glaciers by Maisch (1999), which are thus not included in the map. The manual editing of zone 2 has largely solved these problems. However further improvements would be possible by merging the existing rock glacier inventories in Switzerland and completing a nationwide inventory by mapping hitherto uninvestigated areas. In this way, rock glaciers could be excluded from the automatic mapping of ice-rich ground, allowing to focus on ice-rich talus slopes, which are easier to delimit automatically.

Ice-rich permafrost occurs in the European Alps only in loose rock sediments, so the uncertainty in mapping can be lowered radically by distinguishing loose rock from solid bedrock. Such a dataset does not yet exist on a national scale and in the required accuracy. Existing automatic classification algorithms are not able to perform this differentiation. This problem was also improved by manual editing of zone 2. A refinement of the result would nevertheless be useful.

Kenner and Magnusson (2017) highlighted the influence of the combined effect of lithology and precipitation on ice-rich permafrost. As ice-rich permafrost is less frequent in sedimentary rock areas with high precipitation rates and relatively abundant in drier areas with crystalline or metamorphic lithology, zone 2 will contain more or less permafrost in the respective regions. These regional climate- and lithology induced differences are difficult to implement in a map and must be carefully interpreted by the user.

5.4 Permafrost area in Switzerland

The PGIM indicates a potential permafrost area of 2000 km^2 in the Swiss Alps, which is considerably less than that indicated by the APIM (3710 km^2 (Böckli, 2013)) and also less than on the PPDM (2550 km^2 (Gruber et al. 2006)). To estimate the true permafrost area, Böckli (2013) suggested to consider all areas of the APIM with an index value > 0.5. This results in an area of 2160 km^2 for the APIM. The PGIM includes 830 km^2 in the core area of zone 1 and 600 km^2 in zone 2, of which maximum 90% are expected to include permafrost according to the validation output. This results in an area of ≤ 1400 km^2 of permafrost terrain in the Swiss Alps, which corresponds to 3.4% of the area of Switzerland. For comparison, Keller et al. (1998) gave a value of 4-6 %.

5.5 Ground temperatures and ice content

The advantages of the PGIM are not only its relatively high accuracy and low uncertainty. The zonation allows an estimation of the permafrost temperature, as zone 1 indicates ground temperatures and the ice-rich permafrost in Zone 2, located in lower elevations than zone 1, has typically a temperature a few degrees below to 0°C (PERMOS, 2016). The localisation of ice-rich or warm permafrost is particularly important for engineering purposes as it affects the ground stability and bearing capacity strongest (Bommer et al., 2010). Warm permafrost in rock walls is very sensitive to climate fluctuations and can

The Cryosphere Discuss., https://doi.org/10.5194/tc-2018-235
Manuscript under review for journal The Cryosphere
Discussion started: 7 January 2019

contribute to rock slope instability (Davies et al., 2001;Krautblatter et al., 2013;Gruber and Haeberli, 2007). In cold rock permafrost, specially adapted construction materials are required (Bommer et al., 2008).

Furthermore, the distinction of ice-rich permafrost can be the basis for a more accurate estimation of the potential water resources stored as ground ice in mountains (Jones et al., 2018;Böckli, 2013). Additional information on ground ice content as well as average permafrost thickness in ice-rich permafrost would be necessary for such a calculation.

6 Conclusions

This study presents a new permafrost distribution map for the Swiss Alps but also further corroborates the high predictability of ice-poor permafrost and the need to distinguish it from ice-rich permafrost. This is important for mapping and local modelling, but also for developing scenarios of present, past and future permafrost evolution. We conclude that:

- Ground temperatures can be mapped with a clearly sub-Kelvin accuracy at a national scale at several depths in ice-poor or ice-free ground. It is likely that similar results can be obtained in other world regions using the method presented here.
- A major improvement has been achieved in defining permafrost free areas which can be of particular interest for construction projects.
- The distribution of ice-rich permafrost outside of zone 1 is better predicted by the analysis of mass wasting processes than thermal ones.
- The permafrost and ground ice map PGIM presented here contributes towards an improvement in the accuracy of permafrost mapping in Switzerland.
- The 2 zones on the map give the reader clear information on their meaning (ground temperatures resp. the potential occurrence of excess ice permafrost) rather than a probability value and thus enable easy interpretation with a low uncertainty.
- The future adaptation of the map to higher ground temperatures induced by climate warming in the reference boreholes is easily possible.

Table 1: Reference boreholes provided by 1 - PERMOS (2016), 2 – WSL Institute for Snow and Avalanche Research SLF, 3 - Swiss Federal Office for the Environment FOEN, 4 - University of Lausanne, 5 - ARPA Valle d'Aosta. The uppermost 15 were used for the calculation of ground temperatures in zone 1 of the PGIM. The lowermost 8 were used to demonstrate the failure of this calculation if ice-rich and ice-poor boreholes are not distinguished (Table 3).

Line	Site name & provider	Abbreviation	Ground ice content	Elevation [m a.s.l.]	Longitude (WGS 84)	Latitude (WGS 84)
1	Breithorn [3]	BH	Ice-free	2865	7.81785	46.14010
2	Flüela 0202 [2]	FLU_0202	Ice-free	2501	9.94314	46.74687
3	Tsaté [1]	TSA_0104	Ice-poor	3040	7.54844	46.10904
4	Schilthorn 5200 [1]	SCH_5000	Ice-poor	2910	7.83442	46.55828
5	Stockhorn 6000 [1]	STo_6000	Ice-poor	3410	7.82419	45.98678
6	Les Attelas 3 [4]	ATT_0308	Ice-free	2741	7.27492	46.09659
7	Jungfrau [1]	JFJ_0195	Ice-poor	3590	7.97316	46.54617
8	Gemsstock [1]	GEM_0106	Ice-free	2940	8.61043	46.60125
9	Cima Bianchi 41 [5]	CB41	Ice-poor	3094	45.91906	7.69249
10	Muot da Barba Peider 0196 [1]	MPB_0196	Ice-poor	2946	9.93109	46.49639
11	Muot da Barba Peider 0296 [1]	MPB_0296	Ice-poor	2942	9.93143	46.49657
12	Cima Bianchi 7 [5]	CB7	Ice-poor	3098	45.91920	7.69277
13	Grépillon, upper [5]	GPU	Ice-free	3047	7.05690	45.90990
14	Grépillon, lower [5]	GPL	Ice-free	3000	7.05638	45.90919
15	Matterhorn [1]	MAT_0205	Ice-poor	3288	7.67605	45.98232
16	Flüela 0102 [1]	FLU_0102	Ice-rich	2394	9.94516	46.74792
17	Attelas 0108 [1]	ATT_0108	Ice-rich	2661	7.27307	46.09677
18	Attelas 0208 [1]	ATT_0208	Ice-rich	2689	7.27368	46.09674
19	Corvatsch 0287 [1]	COR_0287	Ice-rich	2672	9.82185	46.42878
20	Lapires 1108 [1]	LAP_1108	Ice-rich	2500	7.28435	46.10611
21	Muragl 0299 [1]	MUR_0299	Ice-rich	2539	9.92735	46.50722
22	Schafberg 0190 [1]	SBE_0190	Ice-rich	2754	9.92631	46.49737
23	Ritigraben 0102 [1]	RIT_0102	Ice-rich	2690	7.84983	46.17469

The Cryosphere Discuss., https://doi.org/10.5194/tc-2018-235
Manuscript under review for journal The Cryosphere
Discussion started: 7 January 2019

Table 2: Validation sites and the zones assigned to them in the permafrost maps PGIM, APIM (Boeckli et al. 2012) and PPDM (Gruber et al. 2006). Type: IMIS - IMIS station, BH - borehole, CS - construction site, RF - rock fall. Data providers: 1 – WSL Institute for Snow and Avalanche Research SLF, 2 - Cremonese et al. (2011), 3 - University of Lausanne, 4 – Swiss Federal Office for the Environment. 5 – University of Fribourg. Zones and probability classes of the maps: see Figures 3-5.

Type[provider]	Name	Permafrost	PGIM/ Temp. (mod)	APIM	PPDM	Elevation [m a.s.l.]	Longitude (WGS 84)	Latitude (WGS 84)
IMIS [1]	Boveire - Pointe de Toules	No	Zone 2	43	Zone 4	2687	7.23722	45.98480
BH[3]	Lapir2	No	Zone 2	76	Zone 2	2559	7.28345	46.10526
IMIS[1]	Saas - Seetal	No	No perm.	No perm.	Zone 1	2477	7.87895	46.17137
IMIS[1]	Trubelboden - Trubelboden	No	No perm.	No perm.	No perm.	2459	7.58558	46.37096
IMIS[1]	Lukmanier - Lai Verd	No	No perm.	63	No perm.	2554	8.78352	46.60416
IMIS[1]	Fully - Grand Cor	No	No perm.	46	No perm.	2602	7.08964	46.19469
IMIS[1]	Bernina - Puoz Bass	No	No perm.	50	No perm.	2629	9.91588	46.44007
IMIS[1]	Gandegg - Gandegg	No	No perm.	72	No perm.	2710	7.76060	46.42926
IMIS[1]	Kesch - Porta d'Es-cha	No	No perm.	66	Zone 1	2727	9.89813	46.62132
IMIS[1]	Gornergrat - Gornergratsee	No	No perm.	98	Zone 5	2952	7.78359	45.98718
BH[2]	Barthélemy les Rochers (Zinal)	No	No perm.	35	Zone 2	2519	7.59812	46.13660
BH[2]	Neue Monte Rosa Hütte (Zermatt)	No	No perm.	93	Zone 1	2866	7.81233	45.95795
IMIS[1]	Zermatt - Alp Hermetje	No	No perm.	No perm.	No perm.	2409	7.70238	45.99799
IMIS[1]	Goms - Treichbode	No	No perm.	No perm.	No perm.	2428	8.22856	46.48912
IMIS[1]	Julier - Vairana	No	No perm.	No perm.	Zone 1	2426	9.69231	46.47850

IMIS[1]	Oberwald - Jostsee	No	No perm.	No perm.	No perm.	2432	8.31595	46.54522
IMIS[1]	Piz Martegnas - Colms da Prasonz	No	No perm.	No perm.	No perm.	2429	9.53739	46.58009
IMIS[1]	Bedretto - Cavanna	No	No perm.	No perm.	Zone 2	2420	8.51112	46.53268
IMIS[1]	Bernina - Motta Bianca	No	No perm.	No perm.	No perm.	2447	10.02920	46.42057
IMIS[1]	Davos - Hanengretji	No	No perm.	No perm.	No perm.	2456	9.77400	46.78885
IMIS[1]	Goms - Bodmerchumma	No	No perm.	10	Zone 2	2439	8.23251	46.42045
IMIS[1]	Taminatal - Wildsee	No	No perm.	59	No perm.	2468	9.39093	46.96836
IMIS[1]	Eggishorn - Flesch	No	No perm.	No perm.	No perm.	2500	8.09170	46.41680
IMIS[1]	Bever - Valetta	No	No perm.	No perm.	No perm.	2512	9.83713	46.53953
IMIS[1]	Samnaun - Ravaischer Salaas	No	No perm.	No perm.	No perm.	2512	10.33833	46.95637
IMIS[1]	Weissfluhjoch	No	No perm.	34	No perm.	2536	9.80911	46.82955
IMIS[1]	Les Attelas - Lac des Vaux	No	No perm.	No perm.	No perm.	2550	7.26988	46.10529
IMIS[1]	Davos - Barentalli	No	No perm.	No perm.	Zone 2	2557	9.81941	46.69890
IMIS[1]	Les Diablerets - Tsanfleuron	No	No perm.	65	No perm.	2584	7.23939	46.31445
IMIS[1]	Anniviers - Tracuit	No	No perm.	No perm.	No perm.	2589	7.65639	46.12116
IMIS[1]	Arolla - Breona	No	No perm.	No perm.	No perm.	2602	7.56205	46.08742
IMIS[1]	Anniviers - Orzival	No	No perm.	No perm.	Zone 4	2641	7.53536	46.18828

The Cryosphere Discuss., https://doi.org/10.5194/tc-2018-235
Manuscript under review for journal The Cryosphere
Discussion started: 7 January 2019

IMIS[1]	Zermatt - Triftchumme	No	No perm.	19	Zone 4	2753	7.72738	46.04217
CS[2]	Speichersee Totalpsee (Davos)	No	No perm.	26	Zone 2	2501	9.81109	46.83724
CS[2]	Herrenabfahrt Corviglia (St. Moritz)	No	No perm.	14	Zone 2	2829	9.80023	46.50610
BH[2]	Catogne (Bovernier)	No	No perm.	21	No perm.	2331	7.10474	46.06012
BH[2]	La Montagnetta (St. Jean/Grimentz)	No	No perm.	0	No perm.	2270	7.55943	46.19472
BH[2]	Barthélemy les Rochers (Zinal)	No	No perm.	0	Zone 2	2519	7.59812	46.13660
BH[2]	Barthélemy les Rochers (Zinal)	No	No perm.	0	Zone 1	2519	7.59812	46.13660
BH[2]	Emshorn (Oberems)	No	No perm.	16	Zone 1	2506	7.67602	46.26670
BH[2]	Emshorn (Oberems)	No	No perm.	0	No perm.	2506	7.67602	46.26670
BH[2]	Felskinnbahn (Saas Fee)	No	No perm.	68	Zone 2	2585	7.91784	46.08137
BH[2]	Flüelapass (Davos)	No	No perm.	18	Zone 2	2500	9.94317	46.74688
BH[2]	Illsee	No	No perm.	0	Zone 2	2359	7.63472	46.25945
BH[2]	Lapires	No	No perm.	97	Zone 4	2650	7.28345	46.10526
IMIS[1]	St. Niklaus - Oberer Stelligletscher	No	Zone 1: 0.4°C	86	Zone 2	2915	7.75054	46.16782
BH[4]	Breithorn	No	Zone 1: 0.7°C	81	Zone 2	2864	7.81785	46.14010
BH[5]	Attelas 3	No	Zone 1: 0.7°C	69	Zone 4	2741	7.27493	46.09660
IMIS[1]	Arolla - Les Fontanesses	No	Zone 1: 0.9°C	83	Zone 4	2857	7.44542	46.02967
IMIS[1]	Finhaut - L'Ecreuleuse	Yes	Zone 2	18	No perm.	2252	6.96409	46.10076
IMIS[1]	Simplon - Wenghorn	Yes	Zone 2	46	No perm.	2424	8.04516	46.17802
IMIS[1]	Piz Lagrev - Tscheppa	Yes	Zone 2	72	Zone 1	2727	9.74488	46.45112

The Cryosphere Discuss., https://doi.org/10.5194/tc-2018-235
Manuscript under review for journal The Cryosphere
Discussion started: 7 January 2019

IMIS[1]	Vinadi - Alpetta	Yes	Zone 2	82	Zone 5	2729	10.44286	46.93178
IMIS[1]	Saas - Schwarzmies	Yes	Zone 2	91	Zone 5	2799	7.97436	46.12436
CS[2]	Gruobtagfeld (Turtmanntal)	Yes	Zone 2	21	No perm.	2375	7.71797	46.20474
CS[2]	Wasserscheide (Davos Parsenn)	Yes	Zone 2	56	Zone 4	2620	9.80255	46.83391
BH[2]	Gentianes	Yes	Zone 2	87	Zone 5	2894	7.30226	46.08383
BH[2]	Mont Dolin (Arolla)	Yes	Zone 2	49	Zone 4	2597	7.46188	46.02634
BH[2]	Mont Dolin, (Arolla)	Yes	Zone 2	30	No perm.	2574	7.46330	46.02634
BH[2]	Ritigraben (Grächen)	Yes	Zone 2	51	Zone 4	2639	7.84983	46.17470
BH[2]	Seetalhorn (Grächen)	Yes	Zone 2	92	Zone 5	2862	7.85911	46.17642
BH[2]	Stafel-Seetalhorn (Grächen)	Yes	Zone 2	36	Zone 4	2457	7.86022	46.18694
BH[2]	Flüelapass (Davos)	Yes	Zone 2	29	No perm.	2500	9.94317	46.74688
BH[2]	Lapires	Yes	Zone 2	61	Zone 2	2505	7.28435	46.10612
BH[2]	Schafberg I	Yes	Zone 2	74	Zone 4	2752	9.92701	46.49655
BH[2]	Schafberg II	Yes	Zone 2	61	Zone 1	2729	9.92387	46.49909
BH[2]	Murtèl-Corvatsch	Yes	Zone 2	83	Zone 1	2666	9.82186	46.42879
BH[2]	Muragl I	Yes	Zone 2	60	Zone 4	2536	9.92784	46.50757
BH[2]	Les Attelas1	Yes	Zone 2	47	Zone 4	2661	7.27308	46.09677
BH[2]	Les Attelas2	Yes	Zone 2	55	Zone 4	2689	7.27369	46.09675
BH[2]	Emshorn (Oberems)	Yes	No perm.	0	Zone 2	2506	7.67602	46.26670
BH[2]	Muot da Barba Peider, lower shoulder	Yes	Zone 1: -0.1°C	81	Zone 4	2791	9.92891	46.49583
RF[2]	Gemsstock (Andermatt)	Yes	Zone 1: -0.2°C	99	Zone 1	2911	8.61043	46.60125
RF[2]	Chrachenhorn (Davos Monstein)	Yes	Zone 1: -0.4°C	91	Zone 5	2830	9.81226	46.68836
BH[2]	Pointe du Tsaté	Yes	Zone 1: -0.4°C	94	Zone 5	3028	7.54696	46.10995
BH[2]	Lagalp (Berninapass)	Yes	Zone 1: -0.4°C	97	Zone 2	Restricted	Restricted	Restricted

The Cryosphere Discuss., https://doi.org/10.5194/tc-2018-235
Manuscript under review for journal The Cryosphere
Discussion started: 7 January 2019

RF[2]	Kärpf (Elm)	Yes	Zone 1: -0.6°C	74	Zone 4	2654	9.08917	46.91611
CS[2]	Scex Rouge (Les Diablerets)	Yes	Zone 1: -0.6°C	93	No perm.	Restricted	Restricted	Restricted
CS[2]	Diavolezza (Berninapass)	Yes	Zone 1: -0.6°C	98	Zone 5	2993	9.96948	46.40975
BH[2]	Schilthorn 51/98	Yes	Zone 1: -0.7°C	100	Zone 4	2910	7.83462	46.55828
CS[2]	Cabane des Vignettes (Arolla)	Yes	Zone 1: -0.9°C	89	Zone 1	3164	7.47555	45.98865
CS[2]	Rothornhütte (Zermatt)	Yes	Zone 1: -0.9°C	98	Zone 4	Restricted	Restricted	Restricted
CS[2]	Rifugio Camosci (Pizzo Cristallina)	Yes	Zone 1: -0.9°C	94	No perm.	2903	8.53667	46.46444
BH[2]	Muot da Barba Peider I	Yes	Zone 1: -1.0°C	99	6	2938	9.93092	46.49647
BH[2]	Arolla, Mt. Dolin	Yes	Zone 1: -1.0°C	99	Zone 5	2862	7.45473	46.02663
BH[2]	Wisse Schijen (Randa)	Yes	Zone 1: -1.2°C	89	Zone 4	3039	7.74832	46.09635
BH[2]	Hörnligrat (Matterhorn, Zermatt)	Yes	Zone 1: -2.0°C	100	6	3288	7.67605	45.98232
BH[2]	Stockhorn 60/00	Yes	Zone 1: -2.7°C	100	Zone 4	3412	7.82420	45.98679
CS[2]	Cabane Dent Blanche (Ferpècle)	Yes	Zone 1: -3.3°C	100	Zone 2	Restricted	Restricted	Restricted
BH[2]	Jungfraujoch South	Yes	Zone 1: -3.9°C	100	Zone 2	3574	7.97306	46.54548
BH[2]	Jungfraujoch North	Yes	Zone 1: -5.2°C	100	Zone 4	3602	7.97319	46.54611
BH[2]	Eggishorn (Fiesch)	Yes	Zone 1: 0.6°C	88	Zone 1	2847	8.09365	46.42638

Table 3: Results of the regression analysis on ground temperature in dependency of elevation and potential solar radiation. Left: Regression analysis used to map the PGIM. Centre: Regression analysis using only the 'coldest thermistor' in boreholes in homogeneous terrain (no ridges). Right: Same approach as in the central column but including the ice-poor boreholes shown in table 1.

	Ice-poor permafrost (213 thermistors in 15 boreholes)	Ice-poor permafrost (coldest thermistor of 10 boreholes)	Ice-poor and ice-rich permafrost together (coldest thermistor of 10 ice-poor and 8 ice-rich boreholes)
Correlation coefficient	0.944	0.998	0.523
Standard error	0.57° C	0.16° C	1.02° C

Acknowledgements

The authors sincerely thank all persons and institutions that supported this work by providing data. A major part of the reference ground temperatures was provided by PERMOS. Paolo Pogliotti (ARPA Valle d'Aosta) and Christophe Lambiel (University of Lausanne) contributed valuable borehole temperature data to the study. Ilja Burn is thanked for checking and manually editing the polygons representing zone 2 of the PGIM and Martin Schneebeli and the Editor Moritz Langer kindly provided constructive comments to the manuscript.

The Cryosphere Discuss., https://doi.org/10.5194/tc-2018-235
Manuscript under review for journal The Cryosphere
Discussion started: 7 January 2019

References

Böckli, L., Brenning, A., Gruber, S., and Noetzli, J.: Permafrost distribution in the European Alps: calculation and evaluation of an index map and summary statistics, The Cryosphere, 6, 807-820, 10.5194/tc-6-807-2012, 2012.

Böckli, L.: Characterizing permafrost in the entire European Alps: spatial distribution and ice content, University of Zurich, Mathematisch-naturwissenschaftliche Fakultät., 2013.

Bommer, C., Keusen, H.-R., and Phillips, M.: Engineering solutions for foundations and anchors in mountain permafrost, 9th International Conference on Permafrost, Fairbanks, Alaska, 2008, 159-163,

Bommer, C., Phillips, M., and Arenson, L. U.: Practical recommendations for planning, constructing and maintaining infrastructure in mountain permafrost, Permafrost and Periglacial Processes, 21, 97-104, 10.1002/ppp.679, 2010.

Cremonese, E., Gruber, S., Phillips, M., Pogliotti, P., Boeckli, L., Noetzli, J., Suter, C., Bodin, X., Crepaz, A., Kellerer-Pirklbauer, A., Lang, K., Letey, S., Mair, V., Morra di Cella, U., Ravanel, L., Scapozza, C., Seppi, R., and Zischg, A.: Brief Communication: "An inventory of permafrost evidence for the European Alps", The Cryosphere, 5, 651-657, 10.5194/tc-5-651-2011, 2011.

Davies, M. C. R., Hamza, O., and Harris, C.: The effect of rise in mean annual temperature on the stability of rock slopes containing ice-filled discontinuities, Permafrost and Periglacial Processes, 12, 137-144, 2001.

Delaloye, R., Reynard, E., Lambiel, C., Marescot, L., and Monnet, R.: Thermal anomaly in a cold scree slope (Creux du Van, Switzerland), Eighth International Conference on Permafrost, Zurich, 2003, 175-180,

Delaloye, R., and Lambiel, C.: Drilling in a low elevation cold talus slope (Dreveneuse, Swiss Prealps), Geophysical Research Abstracts, 9, 10907, 2007.

Deluigi, N., Lambiel, C., and Kanevski, M.: Data-driven mapping of the potential mountain permafrost distribution, Science of The Total Environment, 590, 370-380, 2017.

Gruber, S., and Hoelzle, M.: Statistical modelling of mountain permafrost distribution: local calibration and incorporation of remotely sensed data, Permafrost and Periglacial Processes, 12, 69-77, 2001.

Gruber, S., Hoelzle, M., and Haeberli, W.: Rock-wall temperatures in the Alps: modelling their topographic distribution and regional differences, Permafrost and Periglacial Processes, 15, 229-307, 2004.

Gruber, S., Haeberli, W., Krummenacher, B., Keller, F., Mani, P., Hunziker, G., Hölzle, M., Vonder Mühll, D., Zimmermann, M., Keusen, H.-R., A., G., and Rätzo, H.: Erläuterungen zur Hinweiskarte der potentiellen Permafrostverbreitung in der Schweiz 1:50'000, Swiss Federal Office for the Environment (FOEN), 2006.

Gruber, S., and Haeberli, W.: Permafrost in steep bedrock slopes and its temperature-related destabilization following climate change, Journal of Geophysical Research: Earth Surface, 112, 10.1029/2006JF000547, 2007.

Haberkorn, A., Hoelzle, M., Phillips, M., and Kenner, R.: Snow as a driving factor of rock surface temperatures in steep rough rock walls, Cold Regions Science and Technology, 118, 64-75, 10.1016/j.coldregions.2015.06.013, 2015a.

Haberkorn, A., Phillips, M., Kenner, R., Rhyner, H., Bavay, M., Galos, S. P., and Hoelzle, M.: Thermal Regime of Rock and its Relation to Snow Cover in Steep Alpine Rock Walls: Gemsstock, Central Swiss Alps, Geografiska Annaler: Series A, Physical Geography, 97, 579-597, 10.1111/geoa.12101, 2015b.

Haeberli, W.: Untersuchungen zur Verbreitung von Permafrost zwischen Flüelapass und Piz Grialetsch (Graubünden). Mitteilungen der Versuchsanstalt für Wasserbau, Hydrologie und Glaziologie der ETH Zürich, Zurich, 221 pp., 1975.

Haeberli, W., Hoelzle, M., Dousse, J. P., Ehrler, C., Gardaz, J. M., Imhof, M., F., K., Kunz, P., R., L., and E., R.: Simulation der Permafrostverbreitung in den Alpen mit geographischen Informationssystemen, Schweizerischer Nationalfonds zur Förderung der wissenschaftlichen Forschung, 58, 1996.

Haeberli, W.: Modern Research Perspectives Relating to Permafrost Creep and Rock Glaciers: A Discussion, Permafrost and Periglacial Processes, 11, 290-293, doi:10.1002/1099-1530(200012)11:4<290::AID-PPP372>3.0.CO;2-0, 2000.

Hilbich, C., Hauck, C., Hoelzle, M., Scherler, M., Schudel, L., Völksch, I., Vonder Mühll, D., and Mäusbacher, R.: Monitoring mountain permafrost evolution using electrical resistivity tomography: a 7-year study of seasonal, annual and long-term variations at Schilthorn, Swiss Alps, Journal of Geophysical Research, 113, 10.1029/2007JF000799, 2008.

Hipp, T., Etzelmüller, B., Farbrot, H., Schuler, T. V., and Westermann, S.: Modelling borehole temperatures in Southern Norway – insights into permafrost dynamics during the 20th and 21st century, The Cryosphere, 6, 553-571, 10.5194/tc-6-553-2012, 2012.

Hoelzle, M.: Permafrost occurrence from BTS measurements and climatic parameters in the Eastern Swiss Alps, Permafrost and Periglacial Processes, 3, 143-147, 1992.

Hoelzle, M., Haeberli, W., and Keller, F.: Application of BTS-measurements for modelling permafrost distribution in the Swiss Alps, 6th International Conference on Permafrost, Beijing, China, 1993,

Hoelzle, M., and Haeberli, W.: Simulating the effects of mean annual air-temperature changes on permafrost distribution and glacier size: an example from the Upper Engadin, Swiss Alps., Annals of Glaciology, 21, 399-405, 1995.

Hoelzle, M., Mittaz, C., Etzelmüller, B., and Haeberli, W.: Surface energy fluxes and distribution models of permafrost in European mountain areas: an overview of current developments, Permafrost and Periglacial Processes, 12, 53-68, 2001.

Hoelzle, M., and Gruber, S.: Borehole and ground surface temperatures and their relationship to meteorological conditions in the Swiss Alps, 2008.

Huete, A. R.: A soil-adjusted vegetation index (SAVI), Remote Sensing of Environment, 25, 295-309, 10.1016/0034-4257(88)90106-X, 1988.

Jones, D. B., Harrison, S., Anderson, K., Selley, H. L., Wood, J. L., and Betts, R. A.: The distribution and hydrological significance of rock glaciers in the Nepalese Himalaya, Global and Planetary Change, 160, 123-142, 10.1016/j.gloplacha.2017.11.005, 2018.

Keller, F.: Automated mapping of mountain permafrost using the program PERMAKART within the Geographical Information Systems ARC/INFO, Permafrost and Periglacial Processes, 3, 133-138, 1992.

Keller, F., Frauenfelder, R., Gardaz, J. M., Hoelzle, M., Kneisel, M., Lugon, R., Phillips, M., Reynard, E., and Wenker, L.: Permafrost map of Switzerland, Seventh International Conference on Permafrost, Yellowknife Canada, 1998, 557-562,

Kenner, R., and Magnusson, J.: Estimating the effect of different influencing factors on rock glacier development in two regions in the Swiss Alps, Permafrost and Periglacial Processes, 28, 195-208, 10.1002/ppp.1910, 2017.

Kenner, R., Phillips, M., Hauck, C., Hilbich, C., Mulsow, C., Bühler, Y., Stoffel, A., and Buchroithner, M.: New insights on permafrost genesis and conservation in talus slopes based on observations at Flüelapass, Eastern Switzerland, Geomorphology, 290, 101-113, 10.1016/j.geomorph.2017.04.011, 2017.

Krautblatter, M.: Detection and Quantification of Permafrost Change in Alpine Rock Walls and Implications for Rock Instability, 2009.

Krautblatter, M., Funk, D., and Günzel, F. K.: Why permafrost rocks become unstable: a rock–ice-mechanical model in time and space, Earth Surface Processes and Landforms, 38, 876-887, 10.1002/esp.3374, 2013.

Maisch, M.: Die Gletscher der Schweizer Alpen: Gletscherhochstand 1850, aktuelle Vergletscherung, Gletscherschwund-Szenarien ; [Projektschlussbericht im Rahmen des Nationalen Forschungsprogrammes "Klimaänderungen und Naturkatastrophen", NFP 31], vdf, Hochsch.-Verlag an der ETH, 1999.

Marmy, A., Salzmann, N., Scherler, M., and Hauck, C.: Permafrost model sensitivity to seasonal climatic changes and extreme events in mountainous regions, Environmental Research Letters, 8, 035048, 2013.

PERMOS: Permafrost in Switzerland 2010/2011 to 2013/2014, PERMOS, 85, 2016.

Phillips, M., Zenklusen Mutter, E., Kern-Luetschg, M., and Lehning, M.: Rapid degradation of ground ice in a ventilated talus slope: Flüela Pass, Swiss Alps, Permafrost and Periglacial Processes, 20, 1-14, 10.1002/ppp.638, 2009.

Pruessner, L., Phillips, M., Farinotti, D., Hoelzle, M., and Lehning, M.: Near-surface ventilation as a key for modeling the thermal regime of coarse blocky rock glaciers, Permafrost and Periglacial Processes, 29, 152-163, 2018.

Reynard, E., Lambiel, C., Delaloye, R., Devaud, G., Baron, L., Chapellier, D., Marescot, L., and Monnet, R.: Glacier/permafrost relationships in forefields of small glaciers (Swiss Alps), Proceedings 8th International Conference on Permafrost, Zurich, Switzerland, 2003, 947-952,

Ribolini, A., Guglielmin, M., Fabre, D., Bodin, X., Marchisio, M., Sartini, S., Spagnolo, M., and Schoeneich, P.: The internal structure of rock glaciers and recently deglaciated slopes as revealed by geoelectrical tomography: insights on permafrost and recent glacial evolution in the Central and Western Alps (Italy–France), Quaternary Science Reviews, 29, 507-521, 10.1016/j.quascirev.2009.10.008, 2010.

Russi, T., Ammann, W., Brabec, B., Lehning, M., and Meister, R.: Avalanche Warning Switzerland 2000, in: Early Warning Systems for Natural Disaster Reduction, edited by: Zschau, J., and Küppers, A., Springer Berlin Heidelberg, Berlin, Heidelberg, 569-577, 2003.

Scapozza, C., Lambiel, C., Baron, L., Marescot, L., and Reynard, E.: Internal structure and permafrost distribution in two alpine periglacial talus slopes, Valais, Swiss Alps, Geomorphology, 132, 208-221, 10.1016/j.geomorph.2011.05.010, 2011.

Scherler, M., Hauck, C., Hoelzle, M., and Salzmann, N.: Modeled sensitivity of two alpine permafrost sites to RCM-based climate scenarios, Journal of Geophysical Research: Earth Surface, 118, 780-794, 10.1002/jgrf.20069, 2013.

Staub, B., Marmy, A., Hauck, C., Hilbich, C., and Delaloye, R.: Ground temperature variations in a talus slope influenced by permafrost: a comparison of field observations and model simulations, Geogr. Helv., 70, 45-62, 10.5194/gh-70-45-2015, 2015.

Zenklusen Mutter, E., and Phillips, M.: Active layer characteristics at ten borehole sites in Alpine permafrost terrain, Switzerland, Permafrost and Periglacial Processes, 23, 138-151, 10.1002/ppp.1738, 2012.

Zhang, T.: Influence of the seasonal snow cover on the ground thermal regime: an overview, Reviews of Geophysics, 43, 1-23, 2005.

The Cryosphere Discuss., https://doi.org/10.5194/tc-2018-235
Manuscript under review for journal The Cryosphere
Discussion started: 7 January 2019

Appendix

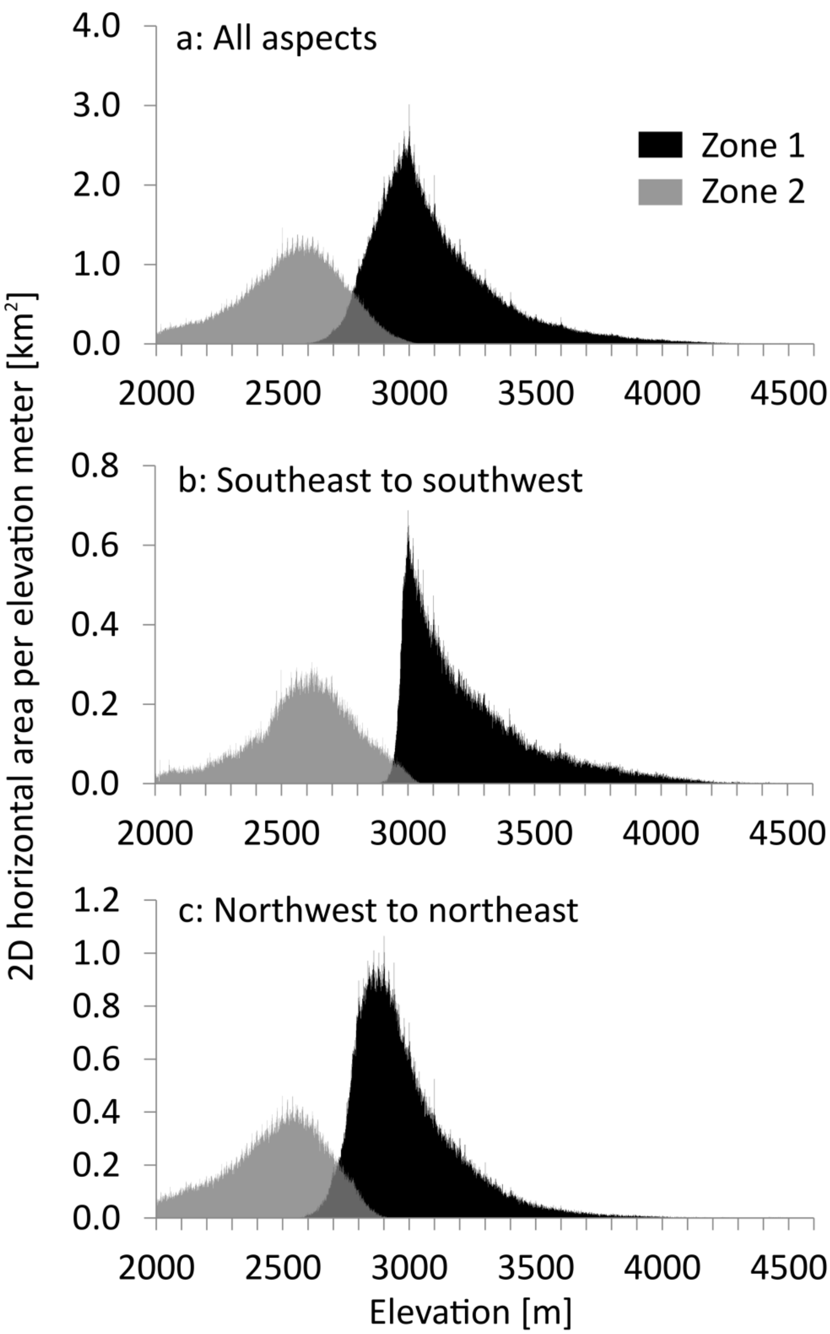

5 **Figure A: Distribution of the PGIM zones 1 (only negative ground temperatures) and 2 over elevation. Part a shows the permafrost zonation over all aspects, part b for the aspects southeast to southwest and part c for aspects ranging between northwest and northeast. The permafrost gap appears between the two map zones.**